IPASJ International Journal of Mechanical Engineering (IIJME)
Web Site: http://www.ipasj.org/IIJME/IIJME.htm
A Publisher for Research Motivation.....
Email: editoriijme@ipasj.org
Volume 3, Issue 8, August 2015
ISSN 2321-6441

Prediction of Power-Law Fluid Flow through an Eccentric Annulus with Inner Cylinder in Rotation using k-ω Turbulence Model

Satish Kumar Dewangan[1], Dr. (Miss) Shobha Lata Sinha[2]

[1]Assistant Professor, Mechanical Engineering Department, National Institute of Technology; Raipur, C.G. (INDIA)

[2]Professor, Mechanical Engineering Department, National Institute of Technology, Raipur, C.G. (INDIA)

ABSTRACT

Situation of flow through annular pipe arises in many practical situations like chemical process plants, heat exchangers, hydraulic transport etc. Also it presents a situation of inhomogeneous fluid flow case. Thus it is one of the important problems in fluid mechanics from practical as well as from theoretical stand point. Many situations consider non-Newtonian flows through an eccentric annulus with inner cylinder in rotation. The present investigation focuses on prediction of turbulent flow through eccentric annulus, using standard k-ω turbulence model. A three dimensional orthogonal hexahedral mesh with suitable boundary conditions & input parameters was taken as computational domain for eccentric annulus. This was solved with SIMPLE algorithm and QUICK up-winding scheme. The Reynolds number was taken as 15000 considering the two inner cylinder rotational speeds of 300 rpm and 600 rpm. The results were validated against the published experimental work of Nouri & Whitelaw (1997). Radial velocity, axial velocity and tangential velocity of fluid were plotted along chosen planes and contours of molecular viscosity as well as turbulence kinetic energy were observed. The relative effects of these velocity components were discussed for critical sections of the model so as to have close observation of the various flow situations present over the cross-section.

Keywords: Power-Law Fluid, Turbulent Flow, Eccentric Annulus, k-ω turbulence model.

NOMENCLACTURE

Notation	Description of variables/Constants
D_H	Hydraulic mean Diameter, 2δ m
e	Eccentricity (Displacement of inner –cylinder axis from outer-cylinder axis), m
e_{max}	Maximum eccentricity, m
k	Consistency Index, Pa-s^n
n	Power-law index
R	Radial distance from axis of inner-cylinder, m
R_i, D_i	Outer radius & diameter of inner-cylinder, m
R_O, D_O	Inner radius & diameter of outer cylinder, m
A	Cross sectional area of annulus of flow, $(\pi/4)$ ($D_O^2 - D_I^2$) m^2
Re	Bulk axial Reynolds number, $2\delta\rho U/\mu_{wall}$
U	Bulk axial velocity, m/s
U_{inlet}	Bulk axial velocity at inlet, m/s
U_a	Axial component of the velocity, m/s
U_t	Tangential component of velocity, m/s
U_r	Radial component of velocity, m/s
U_{rn}	Normalised radial velocity
U_{tn}	Normalised tangential velocity
U_{an}	Normalised axial velocity
r	Radial coordinate, m
z	Axial distance, m
x	Coordinate along axial (i.e. z-direction)
Φ	Angular location with respect to inner cylinder
t	Coordinate along angular direction (i.e. tangential coordinate)
ρ	Fluid Density, kg/m^3
μ	Characteristic Dynamic viscosity for flow, Pa-s
μ_{wall}	μ at wall, Pa-s
ω	Angular velocity of inner cylinder, rad/s
O_1	Centre of inner cylinder (reference centre)

O_2	Centre of the outer cylinder
t	Time coordinate
Υ	Characteristic Shear Rate of flow (s^{-1})
σ_T	Reynolds stress
P	Flow pressure
e_r	Unit vector along radial coordinate
e_t	Unit vector along tangential coordinate
e_a	Unit vector along axial coordinate
$P1_X$	Distance along plane *P1*
$P2_Y$	Distance along plane *P2*
$P3_X$	Distance along plane *P3*
$P1_{nX}$	Normalised values in relation to $P1_X$
$P2_{nY}$	Normalised values in relation to $P2_{nY}$
$P3_{Nx}$	Normalised values in relation to $P3_{nX}$
G_k	Generation of mean kinetic energy due to velocity gradient
G_ω	Generation of specific dissipation rate due to mean velocity gradient
Y_k	Dissipation of mean kinetic energy
Y_ω	Dissipation of specific dissipation rate
Γ_k	Effective diffusivity of mean kinetic energy
Γ_ω	Effective diffusivity of specific dissipation rate
S_k	User defined source terms for *k*
S_ω	User defined source term for ω

1.INTRODUCTION

Flow through concentric and eccentric annulus is a problem of very much practical importance. Such situation arises in many industrial processes like petroleum industries, biomedical engineering applications, Food process industries, Power plants, Heat exchangers etc. A large variety of fluids and industrial applications has been a major motivation for research in annular flow with varying degrees of complexity. An extensive bibliographic list of work on annular flows has been presented by Escudier, Oliveira & Pinho (2002). In the process industries, fluids are being increasingly encountered which do not exhibit Newtonian flow behaviour, that is, the shear rate is not directly proportional to the applied stress. In many engineering design problems, it is important that this non-ideal behaviour be taken into account. Such non-Newtonian fluids should not be regarded as curiosities because many materials which are of considerable industrial importance are highly non- Newtonian in character. (Wilkinson, 1972).

Usual situation occurring in the case of oil well and gas well drilling mud flow is either transition or turbulent flow situations. In the work of Nouri & Whitelaw (1997) three velocity components (axial, radial and tangential) of a Newtonian and a weakly elastic shear-thinning non-Newtonian fluid have been measured in an annulus with an eccentricity of 0.5, a diameter ratio of 0.5, and an inner cylinder rotation of 300 rpm. The results show that the rotation had similar effects on the Newtonian and non-Newtonian fluids, with a more uniform axial flow across the annulus and the maximum tangential velocities in the narrowest gap in both cases. The turbulence intensities in the region of widest gap were not influenced by rotation, increased in the Newtonian fluid, and decreased in the non-Newtonian fluid in the region of the smallest gap.

Cruz and Pinho (2004) has obtained analytical solution of helical flow of fluids in concentric annuli due to inner cylinder rotation as well for Poiseuille flow in a channel skewed by the movement of one plate in span wise direction, which constitutes a simpler solution for helical flow in the limit of very thin annuli. Expressions are derived for the radial variation of the axial and tangential velocities, as well as for the three shear stresses and the two normal stresses using non dimensional number as Reynolds Number and Taylor Number etc. Frigaard and Ngwa (2010) has worked in predicting the rheological properties that are necessary to prevent the annular plug fluid from flowing under the action of buoyancy, or indeed to predict how far the plug material may flow for given rheological properties for annular fluid flow in oil wellbore construction. Mathematically, these flows were modelled using a Hele-Shaw approximation of the narrow annulus. Kelessidis and Bandelis (2004) has presented a critical review of the state-of-art modelling for efficient cutting transport during Coiled-tube drilling, and presented the critical parameters like pump rate, well dimension, fluid sizes, solid loading and hole inclination etc affecting efficient cutting transport. They set up a laboratory system also. Escudier et. al. (2002) reports experimental data for fully developed laminar flow of a shear-thinning liquid through both a concentric and an 80% eccentric annulus with and without centre body rotation. The working fluid was an aqueous solution of 0.1% xanthan gum and 0.1%carboxy-methyl cellulose.

Gavrilov et al. (2011) proposed a numerical algorithm for simulating steady laminar flows of an incompressible fluid in annular channels with eccentricity and rotation of the inner cylinder. The algorithm enabled description of this class of flows for wide ranges of the annular channel and flow parameters. For a series of flows in an annular clearance, these

numerical results were compared with the available analytic solutions and experimental data. The simulated data agree well with the available experimental, analytical, and numerical solutions. Han et al. (2008) investigated hydraulic transport characteristics of a solid-liquid mixture flowing vertically upward where solid particles are carried by non-Newtonian fluids in a slim hole concentric annulus with rotating inner cylinder. Solid volumetric concentration and pressure drops were measured for the various parameters such as angle of inclined annulus, flow rate, and rotational speed of inner cylinder. Aqueous solution of sodium carboxymethyl cellulose (approximately 0.2 - 0.4%) CMC and 5% bentonite solutions were taken for non Newtonian fluid one by one. For both CMC and bentonite solutions, the higher the concentration of the solid particles, the larger the pressure drops become.

Zhiyuan and Baojiang (2009) established the basic hydrodynamic models, including mass, momentum, and energy conservation equations for annular flow with gas hydrate phase transition during gas kick for deep water drilling. They investigated the behaviour of annular multiphase flow with hydrate phase transition by analyzing the hydrate-forming region, the gas fraction in the fluid flowing in the annulus, pit gain, bottom hole pressure, and shut-in casing pressure. Results show that it is possible to move the hydrate-forming region away from sea floor by increasing the circulation rate. The decrease in gas volume fraction in the annulus due to hydrate formation reduces pit gain, which can delay the detection of well kick and increase the risk of hydrate plugging in lines. Caution is needed when a well is monitored for gas kick at a relatively low gas Production rate, because the possibility of hydrate presence is much greater than that at a relatively high production rate. The shut-in casing pressure cannot reflect the gas kick due to hydrate formation, which increases with time.

Kim and Hwang (2003) conducted an experimental investigation concerning the characteristics of vortex flow in a concentric annulus with a diameter ratio of 0.52, whose outer cylinder is stationary and inner one is rotating. Pressure losses and skin friction coefficients have been measured for fully developed flows of water and of 0.4% aqueous solution of sodium carboxy-methyl cellulose (CMC), respectively, when the inner cylinder rotates at the speed of 0-600 rpm. Also, the visualization of vortex flows has been performed to observe the unstable waves.

Podryabinkin and Rudyak (2011) presents results of numerical modelling for analysis of the moment and forces exerted on an eccentrically positioned rotating inner cylinder due to the annular flow between two cylinders with parallel axes. Laminar stationary fully developed flows of Newtonian and power law fluid flows are considered. An impact of annulus geometry, flow regime, and fluid characteristics are studied. The study indicates that the moment exerted on the inner cylinder increases monotonically with the eccentricity. Forces acting on the inner cylinder include pressure and viscous friction. The pressure forces provide a pre-dominant contribution. When eccentricity does not exceed a certain critical value, the radial force pushes the inner cylinder to the channel wall. When eccentricity is large enough, the radial force reverses its sign, and the inner cylinder is pushed away from the outer wall. Circumferential component of the force has always the same direction and induces precession of the inner cylinder. Han, Woo & Hwang (2009) experimentally studied solid-liquid mixture upward hydraulic transport of solid particles in vertical and inclined annuli with rotating inner cylinder. Effect of annulus inclination and drill pipe rotation on the carrying capacity of drilling fluid, particle rising velocity, and pressure drop in the slim hole annulus have been measured for fully developed flows of water and of aqueous solutions of sodium carboxymethyl cellulose (CMC) and bentonite, respectively. For higher particle feed concentration, the hydraulic pressure drop of mixture flow increases due to the friction between the wall and solids or among solids.

Solution methodology adopted for these various researches were based on the consideration that of turbulent flow of the non-Newtonian fluid or multiphase fluids in the annular flow geometry are often encountered in the oil well drilling. Usually the solution methodologies have been the experimental and sometimes the numerical based methodologies.

In computational solution procedure, while solving such problems selection of proper turbulence model, selection of proper pressure – velocity coupling resolution method and type of descretization schemes for flow are very essential.

The choice of turbulence model depends on the considerations such as the physics encompassed in the flow, the established practice for a specific class of problem, the level of accuracy required, the available computational resources and the amount available for the simulations. In order to make the most appropriate choice of the model for a particular application, one must understand the capability and limitations of the various turbulence models.

Turbulence modelling done by k-ω model are of two varieties namely standard k-ω turbulence model and Shear Stress Transport (SST) k-ω turbulence model. Both models have similar forms, with transport equations for k and ω. The major ways in which the SST model differs from the standard model are as follows:

a. Gradual change from standard k-ω model in the inner region of the boundary layer to a high Reynold number version of the k-ε model in the outer part of the boundary layer

b. Modified turbulent viscosity formulation to account for the transport effects of the principal turbulent shear stress.

The standard k-ω model is based on Wilcox k-ω model, which incorporates modifications for low-Reynolds-number effects, compressibility and shear flow spreading. The Wilcox model predicts free shear flow spreading Rates that are in close agreement with the measurement for far wakes, mixing layers and plane, round and radial jets and is thus applicable to wall-bounded flows and free shear flows. The standard k-ω model is an empirical model based on model

transport equations for the turbulence kinetic energy (k) and the specific dissipation rate (ω), which can also be thought of as the ratio of ε to k. As the k-ω model has been modified over the years, production terms have been added to both the k and ω equations, which have improved the accuracy of the model for the prediction of the free shear flows.(ANSYS user guide and manuals)

ANSYS-FLUENT 12 offers nine different turbulence models to capture the transition & turbulence effects in the flow. Since the present flow situation possibly lies in the transition flow situation thus standard *k–ω* (Turbulence Kinetic Energy – Specific dissipation rate) model was adopted. This incorporated the modifications for shear flow corrections and low Reynolds number effects (within turbulence). (ANSYS user guide and manuals)

The objective of the present study is to investigate the flow prediction effectiveness of standard *k-ω* turbulence model for case of eccentric annulus (Refer Table 1 for model details) non-Newtonian flow with inner cylinder rotation. The results if it has been verified by comparing them with that of experimental data for the case considered. Three dimensional and two dimensional (mid-plane of the annulus normal to the annulus axis) representation of the geometry is shown in Figure 1 & Figure 2 respectively.

Table 1. Model Details

Cylinder Diameter (D_1)	20 mm	Axial dimension for the cylinders	10 mm
Outer cylinder Diameter (D_o)	40.3 mm	Inner cylinder is in clockwise rotation with 300 rpm.	
Axial dimension for the cylinders	10 mm	Outer cylinder is fixed.	
Maximum Eccentricity (e_{max})	5.15 mm	Centre of the inner cylinder is taken as reference Centre for measurement of the eccentricity.	
Max hydraulic mean diameter $(D_h)_{max}$	20.3 mm		

Flow is considered to be three dimensional, incompressible, steady & in transition with Bulk axial Reynolds number (Re) equal to 15000. The flow direction is along positive z-axis, through the eccentric annulus of flow between the cylinders. Axial mass flow rate (m) & axial bulk velocity (U) corresponding to the chosen Reynolds number was 4.275 kg/s and 4.433m/s, which were calculated using the following relations;

Axial Bulk velocity; $U = (R_e\, D_H\, \rho) / \mu_{wall}$; and

Axial mass flow rate; $m = U\ A\ \rho$.

Where $A = (\pi/4)\ (D_O^2 - D_I^2)$, and $\mu_{wall} = 6 \times 10^{-3}$ measured experimentally by Nouri& Whitelaw (1997)

The numerical formulation is based on the finite volume method as implemented in ANSYS-FLUENT 12. SIMPLE algorithm has been applied for dealing with pressure velocity coupling.

2.MATHEMATICAL FORMULATION

2.1. Governing Equations

In the present work, flow has been modelled as three dimensional, incompressible, Transition flow of Non-Newtonian fluid. ANSYS-FLUENT solves the problem using conservation equations as guideline. Flow of fluid is governed by the Navier–Stokes equation and continuity equations. The coordinate-free time averaged form of the Navier-Stokes equations (Muralidhar & Biswas, 2005) is being given below;

$$\rho\left(\frac{\partial \bar{U}}{\partial \tau} + \bar{U}.\nabla\bar{U}\right) = -\nabla p + \mu\,\nabla^2\bar{U} + \nabla.\sigma_T \qquad (1)$$

Time averaged velocity components of turbulent flow satisfy the same Navier-Stokes equation as for laminar flow, provided the laminar stresses are increased by additional stress known as apparent stresses of turbulent flow or Reynolds stresses. These are given by symmetric stress tensor as below;

$$\sigma_T = \begin{bmatrix} \overline{U_r^2} & \overline{U_r U_t} & \overline{U_r U_a} \\ \overline{U_r U_t} & \overline{U_t^2} & \overline{U_t U_a} \\ \overline{U_r U_a} & \overline{U_t U_a} & \overline{U_a^2} \end{bmatrix} \qquad (2)$$

Details of velocity vector *U* and Del operators in radial coordinates are as below;

$$\bar{U} = \bar{U}_r e_r + \bar{U}_t e_t + \bar{U}_a e_a\ ;$$

$$\nabla = \left(e_r\frac{\partial}{\partial r} + \frac{e_t}{r}\frac{\partial}{\partial t} + e_a\frac{\partial}{\partial a}\right) \qquad (3)$$

IPASJ International Journal of Mechanical Engineering (IIJME)
Web Site: http://www.ipasj.org/IIJME/IIJME.htm
A Publisher for Research Motivation..... Email: editoriijme@ipasj.org
Volume 3, Issue 8, August 2015 ISSN 2321-6441

$$\nabla^2 = \nabla.\nabla = \left(\frac{\partial^2}{\partial r^2} + \frac{1}{r}\frac{\partial}{\partial r} + \frac{1}{r^2}\frac{\partial^2}{\partial t^2} + \frac{\partial^2}{\partial a^2}\right) \quad (4)$$

$$\nabla^2 \bar{U} = (\nabla^2 \bar{U}_r, \nabla^2 \bar{U}_t, \nabla^2 \bar{U}_a) + \frac{1}{r^2}\frac{\partial^2}{\partial t^2}\bar{U} \quad (5)$$

The second term is;

$$\left(\frac{\partial^2 \bar{U_r}}{\partial t^2} - U_r - 2\frac{\partial \bar{U_t}}{\partial t}\right)e_r + \left(\frac{\partial^2 \bar{U_t}}{\partial t^2} + 2\frac{\partial \bar{U}_r}{\partial t} - \bar{U}_t\right)e_t \quad (6)$$

The nonlinear acceleration term would be;

$$\bar{U}.\nabla\bar{U} = e_r\left(\bar{U}r\frac{\partial \bar{U}_r}{\partial r} + \frac{U_t}{r}\frac{\partial \bar{U}_r}{\partial t} - \frac{\bar{U}_t^2}{r} + U_a\frac{\partial \bar{U}_r}{\partial a}\right) + e_t\left(\bar{U}r\frac{\partial \bar{U}_t}{\partial r} + \frac{\bar{U}_r\bar{U}_t}{r} + \frac{\bar{U}_t}{r}\frac{\partial \bar{U}_t}{\partial t} + U_a\frac{\partial \bar{U}_t}{\partial a}\right) + e_a\left(\bar{U}r\frac{\partial \bar{U}_a}{\partial r} + \frac{U_t}{r}\frac{\partial \bar{U}_a}{\partial t} + U_a\frac{\partial \bar{U}_a}{\partial a}\right) \quad (7)$$

The continuity equation for the incompressible fluid is given as under;

$$\nabla.\bar{U} = \left(\frac{\partial \bar{U}_r}{\partial r} + \frac{\bar{U}_r}{r} + \frac{1}{r}\frac{\partial \bar{U}_t}{\partial t} + \frac{\partial \bar{U}_a}{\partial a}\right) = 0 \quad (8)$$

Writing the Navier–Stokes equations in this form, allows the flexibility to use arbitrary non-Newtonian fluid model. Energy Conservation equation will not play any role since thermal parameters are not varying.

2.2. Non-Newtonian Fluid Models

ANSYS-FLUENT provides four options for modelling non-Newtonian flows: (a) power law model; (b) Carreaau model for pseudo-plastics; (c) Cross model and (d) Herchel - Bulkey model for Bingham plastics. The test fluid is of Non-Newtonian type. It has been described by power law model and represented by (when temperature is not involved in the case under study) the following equation;

$$\mu = K\ \gamma^{n-1} \quad (9)$$

Where viscosity μ has upper & lower limits as mentioned below;

$$\mu_{min} < \mu < \mu_{max}$$

Here, *k* is the measure of the average viscosity of the fluid (the consistency index); *n* is a measure of the deviation of the fluid from Newtonian state (the power law index). If viscosity computed from the power law crosses these maximum or minimum limits then extreme value of that side will be used instead for calculation. The value of n determines the class of the fluid:

n = 1 -------- Newtonian Fluid
n> 1 ---------- Shear thickening (dilatants fluid)
n< 1 ---------- Shear thinning (pseudo plastics)

Input parameter values for non-Newtonian fluid are already mentioned in the Table 2.

Table 2: Non-Newtonian power law parameters

Power law index *(n)*	0.75	**consistency index *(k)***	0.044
Minimum Viscosity Limit (μ_{min})	0.0001kg/m-s	**Maximum Viscosity Limit (μ_{max})**	1000 kg/m-s
Reference Temperature		310 *K*	

The values of these non-Newtonian power law parameters for test fluid used in this study were obtained from the data prescribed by Nouri& Whitelaw (1997).

2.3. Turbulence modelling by *k-ω* Model

The turbulence kinetic energy, k, and the specific dissipation rate, ω, are obtained from the following transport equations (in tensor form) for the standard k-ω model:

$$\frac{\partial}{\partial \tau}(\rho k) + \frac{\partial}{\partial x_i}(\rho k u_i) = \frac{\partial}{\partial x_j}\left(\Gamma_k \frac{\partial k}{\partial x_j}\right) + G_k - Y_k + S_k \quad (10)$$

And

$$\frac{\partial}{\partial \tau}(\rho \omega) + \frac{\partial}{\partial x_i}(\rho \omega u_i) = \frac{\partial}{\partial x_j}\left(\Gamma_\omega \frac{\partial \omega}{\partial x_j}\right) + G_\omega - Y_\omega + S_\omega \quad (11)$$

The effective diffusivities for the *k-ω* model are given by;

$$\Gamma_k = \mu + \frac{\mu_t}{\sigma_k} \text{ and } \Gamma_\omega = \mu + \frac{\mu_t}{\sigma_\omega} \quad (12)$$

Where σ_k and σ_ω are the turbulent prandtle numbers for *k* and *ω*, respectively. The turbulent viscosity, μ_t, is computed by combining *k* and *ω* as follows:

IPASJ International Journal of Mechanical Engineering (IIJME)
Web Site: http://www.ipasj.org/IIJME/IIJME.htm
A Publisher for Research Motivation..... Email: editoriijme@ipasj.org
Volume 3, Issue 8, August 2015 ISSN 2321-6441

$$\mu_t = \alpha^* \frac{\rho k}{\omega} \qquad (13)$$

2.4. Low -Reynolds-Number-Correction

The coefficient α^* damps the turbulent viscosity causing Low-Reynolds-Number correction. It is given by;

$$\alpha^* = \alpha_\infty^* \left(\frac{\alpha_o^* + \frac{Re_t}{R_k}}{1 + \frac{Re_t}{R_k}} \right) \qquad (14)$$

Where;

$$Re_t = \frac{\rho k}{\mu \omega}; R_k = 6; \alpha_o^* = \beta_i/3; \beta_i = 0.072$$

Note that, in the high-Reynolds-number form of the *k*-ω model, $\alpha_0^* = \alpha_0^* = 1$.

2.5. Modelling the Turbulence Production

Production of turbulent kinetic energy;

$$G_k = -\overline{\rho u_i u_j} \frac{\partial u_j}{\partial x_i} \qquad (15)$$

Production of ω is given by;

$$G_\omega = \alpha \frac{\omega}{k} G_k \qquad (16)$$

The coefficient α is given by;

$$\alpha = \frac{\alpha_\infty}{\alpha^*} \left(\frac{\alpha_0 + Re_t/R_\omega}{1 + Re_t/R_\omega} \right) \qquad (17)$$

Where $R_\omega = 2.95.\alpha^*$ and Re_t are given by previous relations. Not that, in the high Reynolds number form of *k*-ω model, $\alpha = \alpha_\infty = 1$.

2.6. Modelling the Turbulent Dissipation

Dissipation of *k* is given by;

$$Y_k = \rho \beta^* f_{\beta^*} k\omega \qquad (18)$$

Where

$$f_{\beta^*} = \begin{cases} 1 & \chi_k \leq 0 \\ \frac{1+680\,\chi_{k^2}}{1+400\,\chi_{k^2}} & \chi_k > 0 \end{cases} \qquad (19)$$

$$\chi_k = \frac{1}{\omega^3} \frac{\partial k}{\partial x_j} \frac{\partial \omega}{\partial x_j} \qquad (20)$$

And

$$\beta^* = \beta_i^* [1 + \zeta^* F(M_t)]; \beta_i^* = \beta_\infty^* \left(\frac{\frac{4}{15} + \left(\frac{Re_t}{R_\beta}\right)^4}{1 + \left(\frac{Re_t}{R_\beta}\right)^4} \right); \zeta^* = 1, R_\beta = 8 \text{ and } \beta_\infty^* = 0.09. \qquad (21)$$

2.7. Dissipation of ω

The dissipation of ω is given by

$$Y_\omega = \rho \beta f_\beta \omega^2 \qquad (22)$$

Where

$$f_\beta = \frac{1+70\chi_\omega}{1+80\chi_\omega}; \chi_\omega = \left| \frac{\Omega_{ij}\Omega_{jk}S_{ki}}{(\beta_\infty^* \omega)^3} \right| \qquad (23)$$

IPASJ International Journal of Mechanical Engineering (IIJME)
Web Site: http://www.ipasj.org/IIJME/IIJME.htm
A Publisher for Research Motivation..... Email: editoriijme@ipasj.org
Volume 3, Issue 8, August 2015 ISSN 2321-6441

Vorticity tensor;
$$\Omega_{ij} = \frac{1}{2}\left(\frac{\partial u_i}{\partial x_j} - \frac{\partial u_j}{\partial x_i}\right) \quad (24)$$

Strain rate tensor;
$$S_{ki} = \frac{1}{2}\left(\frac{\partial u_i}{\partial x_k} + \frac{\partial u_k}{\partial x_i}\right) \quad (25)$$

3.NUMERICAL FORMULATION

In the present work, three dimensional orthogonal mesh was used with total 20000 hexahedral cells. Two dimensional representation of the grid is shown in the Figure 3.

The following Boundary conditions have been specified for solving the different parameters in the domain;

a. Periodic boundary condition along axial direction at the end faces, with mass flow rate input at z=0;
b. Moving wall boundary condition at the inner wall with clockwise rotation at constant angular velocity ω; and
c. Stationary wall boundary condition at the outer wall.

No slip conditions are applicable at the both walls. The Mesh, model details and boundary conditions were directly taken from the ANSYS user guide & manual. SIMPLE algorithm has been used for pressure velocity coupling. ANSYS – FLUENT 12uses a multi-grid scheme to accelerate the convergence of the solver by computing the corrections on a series of coarse grid levels. The use of multi-grid scheme can greatly reduce the number of iterations and the computational time required to obtain the converged solution. A residual convergence of 10^{-6} has been obtained for the governing variables viz, mass balance, and velocity components of the flow, k and ω. Under relaxation parameters were kept moderate and constant throughout the solution as mentioned in Table 3 below.

Table 3: Under Relaxation Parameters

Parameters	Value	Parameters	Value
Pressure	0.3	Turbulent Kinetic Energy	0.8
Momentum	0.7	Turbulent Viscosity	1
Density	1	Specific Dissipation Rate	0.8
Body Forces	1	Energy	1

For representation of the results, the calculated values will be displayed on defined planes p1, p2 and p3. The three planes are at locations like 3 o'clock, 12 o' clock and 9 o'clock corresponding to analogy with hour-arm of watch with respect to geometry under study. These locations are depicted in the Figure 4 and Table 4 as below.

Table 4: Coordinate Locations of p1, p2 and p3

Plane	Coordinate	Min Extent (m)	Max Extent (m)
P1	X	0.01 m	0.015 m
	Y	0.00 m	0.00 m
	Z	0.005 m	0.005 m
P2	X	- 0.00515 m	- 0.00515 m
	Y	0.008566585 m	0.02015 m
	Z	0.005 m	0.005 m
P3	X	- 0.0253 m	- 0.01m
	Y	0.00 m	0.00 m
	Z	0.005 m	0.005 m

The results obtained were normalised only for the purpose of plot presentation of the results and that only of the velocity values. All velocity values were normalised with respect to inlet velocity as given below;

$$U_{an} = \frac{U_a}{U_{inlet}}; U_{tn} = \frac{U_t}{U_{inlet}}; \; and \, U_{rn} = \frac{U_r}{U_{inlet}}. \quad (26)$$

The following distances along reference planes p1, p2 and p3 for plotting were normalised with respect to the dimension of eccentricity along these respective planes:

$$p1_{nX} = \frac{p1_{X(max)} - p1_X}{p1_{X(max)} - p1_{X(min)}} = \frac{0.015 - p1_X}{0.005} \quad (27)$$

$$p2_{nY} = \frac{p2_{Y(max)} - p2_Y}{p2_{Y(max)} - p2_{Y(min)}} = \frac{0.02015 - p2_Y}{0.012} \quad (28)$$

$$p3_{nX} = \frac{p3_X - p3_{X(\min)}}{p3_{X(max)} - p3_{X(min)}} = \frac{p3_X - (-0.0253)}{0.0153} \quad (29)$$

Here, subscripts 'max' and 'min' indicate the respective maximum and minimum values as mentioned in the Table 4.

4.RESULTS AND DISCUSSION

The results being presented for the case of non-Newtonian fluid flow through the eccentric annulus for two rotational speeds of the inner cylinders at 300 rpm and 600 rpm. These results were obtained for a case of 15000 Reynolds number and 5.15 mm eccentricity with outer cylinder is fixed and inner cylinder in anticlockwise rotation. Figures 5 to 12 indicate the contour plots and Figures 13 to 17 indicate the variation of the velocity values along the defined planes p1, p2 and p3.

Figure 5 and 6 shows the contour of velocity magnitude for 300 and 600 rpm respectively. Due to higher speed of rotation in the anticlockwise sense the higher speed of core portion is pulled towards inside the narrow gap zone of the eccentric annulus. Axial velocity has the major contribution in the velocity magnitude and thus maximum of the velocity magnitude is lying in the wider zone.

Figure 7 and 8 represents the contour plots variation of turbulent kinetic energy for 300 rpm and 600 rpm anticlockwise inner cylinder rotation respectively. Highest values of the turbulent kinetic energy (TKE) are lying near the walls of inner and outer cylinders in the zone between p3 and p1 planes. At these potions total velocity magnitude values are very small (as obvious from the contours). Lowest values of the TKE are lying in the approximately central core of the annulus. Thickness of the core carrying lower values of TKE is at the delivery side of the narrow gap of the annulus near to the plane p2. Turbulence kinetic energy (TKE) is the mean kinetic energy per unit mass associated with eddies in turbulent flow. Physically, the turbulence kinetic energy is characterised by measured root-mean-square (RMS) velocity fluctuations. In Reynolds-averaged Navier Stokes equations, the turbulence kinetic energy can be calculated based on the closure method, i.e. a turbulence model. Generally, the TKE can be quantified by the mean of the turbulence normal stresses:

$$k = \frac{1}{2}\{\overline{(U_a')^2} + \overline{(U_a')^2} + \overline{(U_a')^2}\} \quad (30)$$

Normal stress values being very small (as the fluctuating components of velocities being very small) turbulence kinetic energy will be small or vice versa. As indicated by the turbulence kinetic energy contours, Figure 7 and 8, being maximum near walls and reduces to minimum while proceeding towards middle portions of the eccentric gap at whichever radial direction considered. This shows that at these portions normal stress values and so fluctuating components of velocities and thus shear stress values will be maximum or minimum at those respective portions of the flow field.

Figure 9 and 10 represents the contour of molecular viscosity variation for 300 rpm (anticlockwise) and 600 rpm (anticlockwise) respectively. Molecular viscosity value is approaching its higher values in the central core band portion of the eccentric annulus. The peak value of it is lying within this band at locations just after the plane p3 and just before plane p2, considering in anticlockwise way. The featured variation of the molecular viscosity is opposite to that of TKE.

Figure 11 and 12 represents turbulent viscosity contours for 300 rpm and 600 rpm respectively. From the plots it can be seen that the values are higher near the walls in proximity region of the plane p3. Lowest values of the turbulent viscosity are falling at the walls of inner and outer cylinders, whereas the moderate values of it is lying at the central core region of the narrowest gap of the eccentric annulus. For increase in the speed of rotation of the inner cylinder the highest values of turbulent viscosity shifts towards the inner cylinder wall whereas those near the outer cylinder slowly begins to dissipate.

Figure 13 and 14 represents the axial, tangential and radial velocity variation plots along p2 plane at 600 rpm and along p1 plane at 300 rpm respectively. Velocity values are presented in the normalised values and the distance along the planes (plotted on x-axis) are also shown in normalised form. Traversing along the x-axis signifies proceeding from outer cylinder towards the inner cylinder. Figure 15, 16 and 17 presents the variation of tangential and radial velocity variation along planes p1, p2 and p3 respectively for 300 rpm and 600 rpm inner cylinder rotational speeds.

Figure 13 and 14 are showing the similar relative trends between axial, tangential and radial velocity value. Magnitude values are different as are for the different planes and speed values. These Figures are signifying the dominance of axial velocity values in the total flow velocity, as compared to that of tangential and radial velocity. Lateral mixing and turbulence effects are caused by the tangential and radial velocities which are produced by the rotation of the inner cylinder. With increase in speed of rotation, turbulence values will go up but nonetheless in either situation radial velocity values have very less contribution in the lateral turbulence values, as compared to the tangential velocity.
Figure 15 presents variation of the tangential velocity and radial velocity along the plane p1 for 300 rpm and 600 rpm rotational speeds of the inner cylinder. This reflects the effect of increased speed of rotation of the inner cylinder on these velocity values. Although tangential velocity is increasing with increase in rotation speed, but radial velocity values experience almost very small effects of the speed of rotation.
Figure 16 and 17 presents the effects of increased speed of rotation on tangential velocity as well as radial velocity along plane p2 and plane p3 respectively. From both of these plots, similar conclusions can be drawn that the radial velocity value experiences very less effects of the increased rotation of speed throughout the cross section, as compared the effects on the tangential velocity values.

5.VALIDATION

The predicted flow field is validated against the experimental data by Nouri& Whitelaw (1997). For this, axial velocity (Ua) and tangential velocity (Ut) values were chosen. These were plotted along the three specified planes p1, p2 and p3 with respect to geometry under study. These locations are depicted & detailed in the Figure 4 and Table 4. All velocity values and the specified planes have been normalised (already discussed) for the representation.
Figure 18 shows that the comparison between experimental and numerical result for variation of the axial velocity in the annular gap along the plane p1. There is qualitative match found between the experimental and numerical solutions, and have same trend of variation of axial velocity. Figure 19 is representing the comparison between the Experimental and Numerical results for variation of the tangential velocity along the plane p1. Results by the two methods are following the same trend of variation of tangential velocity values. Both results are satisfying the physical situation of the problem as well.
Figures 20-21 and Figures 22- 23 are representing the tangential velocity variation along planes p2 and p3 respectively for experimental and numerical results (by QUICK scheme). By visual examination a qualitative match in the trend of velocity variation can be seen in these results also. The computed and experimental results are observed to be in good agreement.

6.CONCLUSION

Present work concerns the prediction of k-ω turbulence model for flow through the eccentric annulus. In this work, for a Reynolds number of 15000 and eccentricity of 5.15 mm, two speeds of rotation 300 rpm and 600 rpm were studied. ANSYS-Fluent version 12.0 was used by taking the option of k-ω model in the software. Validation presented at the end of the work signifies the capability of the methodology and the numerical tool for the case considered. From the results it can be concluded that to increase the radial velocity component, mere increase in the speed of inner cylinder will not be enough. Increase in the speed of inner cylinder is helpful for gaining enhancement in the tangential velocity values only. Thus some additional changes in the geometry of the inner cylinder for example some projected part can be attached at the outer portion of the inner cylinder.

7.ACKNOWLEDGEMENT

Authors acknowledge the cooperation extended by authorities of National Institute of Technology, Raipur (C.G.) INDIA for providing the licensed commercial software code ANSYS FLUENT (ANSYS Academic Research CFD version 12) and Tecplot Academic Suit Software package for plotting some of the diagrams.

REFERENCES

[1] ANSYS Academic Research CFD version 12 User Guide & Manuals.
[2] Cruz D.O.A.&Pinho F.T. (2004), Skewed Poiseuille –Couette Flow of sPTT Fluids in concentric annuli and channels, Journal of Non-Newtonian Fluid Mech. 12:1–14.
[3] Escudier M. P., Oliveira P. J., Pinho F. T. & Smith S. (2002), Fully Developed Laminar Flow of Non-Newtonian liquids through annuli: Comparison of numerical calculations with experiments, Experiments in Fluids 33:101 – 111.

[4] Escudier M. P., Oliveira P.J. & Pinho F. T. (2002), Fully developed laminar flow of purely viscous non- Newtonian liquids through annuli, including the effects of eccentricity and inner-cylinder rotation. International Journal of Heat and Fluid Flow 23:52–73.
[5] Frigaard I. A. & Ngwa G. A. (2010), Slumping Flows in Narrow Eccentric Annuli: Design of Chemical Packers and Cementing of Subsurface Gas Pipelines, Transport in Porous Media, Springer Science 83:29–53.
[6] Gavrilov A. A., Minakov A.V., Dekterev A. A.&Rudyak V. Ya. (2011), A Numerical Algorithm for Modeling Laminar Flows in an Annular Channel with Eccentricity, Journal of Applied and Industrial Mathematics, 5, 4,559–568.
[7] Han S. M., Kim Y. J., Woo N. S. & Hwang Y. K. (2008), A study on the solid-liquid Two phase helical flow in an inclined annulus, Journal of Mechanical Science and Technology, 22:1914-1920.
[8] Han S. M., Woo N. S. & Hwang Y. K. (2009), Solid-liquid mixture flow through a slim hole annulus with rotating inner cylinder, Journal of Mechanical Science and Technology, 23:569-577.
[9] Kelessidis V. C. & Bandelis G. E. (2004), Flow Pattern and Minimum Suspension Velocity for Efficient Cuttings Transport in Horizontal and Deviated Wells in Coiled Tube Drilling, Drilling and Completion, Society of Petroleum Engineers.
[10] Kim Y. J. & Hwang Y. K. (2003), Experimental Study on the Vortex Flow in a Concentric Annulus with a rotating inner cylinder, KSME International Journal, 17, 4,562-570.
[11] Muralidhar K. & Biswas G. (2005),Advanced Engineering Fluid Mechanics, Second Edition, Narosa Publishing House Pvt. Ltd.
[12] Nouri J. M. & Whitelaw J. H. (1997), Flow of Newtonian and non-Newtonian fluids in an eccentric annulus with rotation of inner cylinder, International Journal of Heat and Fluid Flow, 18:236-246.
[13] Podryabinkin E. V. & Rudyak V. Ya. (2011), Moment and Forces Exerted on the Inner Cylinder in Eccentric Annular flow, Journal of Engineering Thermo physics, 20, 3, 320–328.
[14] Wilkinson W. L. (1972), Non-Newtonian Flow and Heat Transfer, Proceedings of the Institution of Mechanical Engineers, 109-116.
[15] Zhiyuan W. &Baojiang S. (2009),Annular multiphase flow behaviour during deep water drilling and the effect of hydrate phase transition; Petroleum and Science Technology, 6:57-63.

LIST OF FIGURES

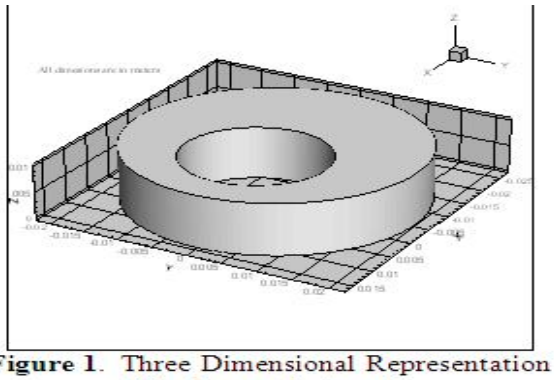

Figure 1. Three Dimensional Representation of the Eccentric Annulus

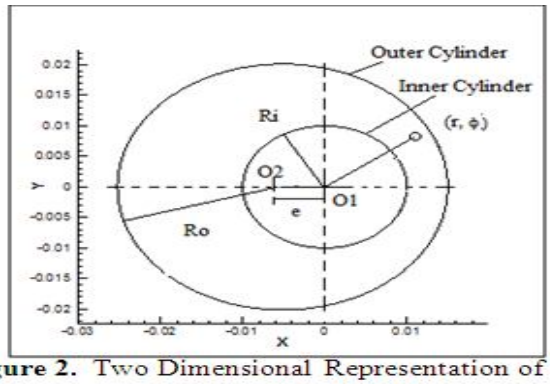

Figure 2. Two Dimensional Representation of the Eccentric Annulus

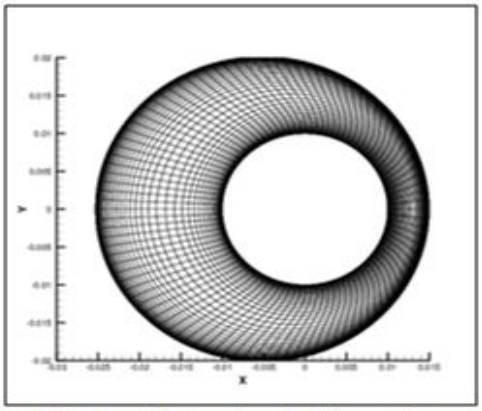

Figure3. Two Dimensional View of eccentric Annulus mesh

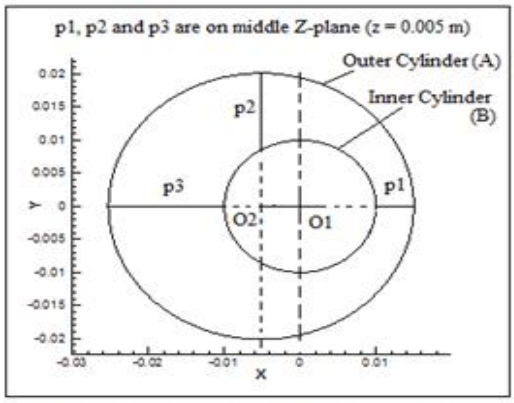

Figure 4. Representation of reference locations p1, p2 and p3 for eccentric annulus model

IPASJ International Journal of Mechanical Engineering (IIJME)
Web Site: http://www.ipasj.org/IIJME/IIJME.htm
A Publisher for Research Motivation.....
Email: editoriijme@ipasj.org
Volume 3, Issue 8, August 2015
ISSN 2321-6441

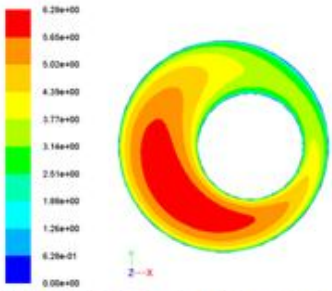

Figure 5. Velocity Magnitude (m/s) contours for Re#15000, eccentricity (5.15 mm), inner rotation (300 RPM) and outer cylinder fixed

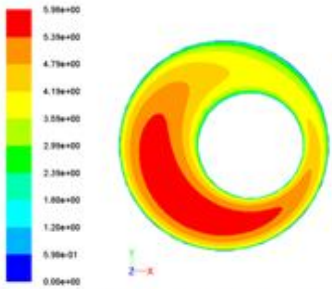

Figure 6. Velocity Magnitude (m/s) contours for Re#15000, eccentricity (5.15 mm), inner rotation (600 RPM) and outer cylinder fixed

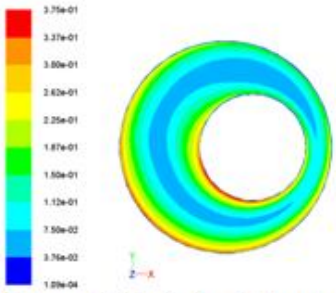

Figure 7. Turbulent Kinetic Energy (m2/s2) contours for Re#15000, eccentricity (5.15 mm), inner rotation (300 RPM) and outer cylinder fixed

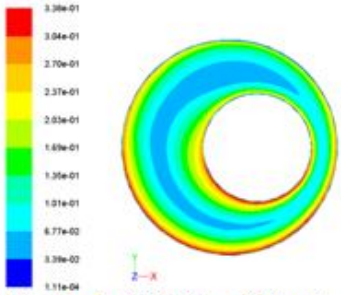

Figure 8. Turbulent Kinetic Energy (m2/s2) contours for Re#15000, eccentricity (5.15 mm), inner rotation (600 RPM) and outer cylinder fixed

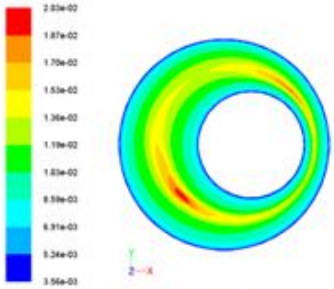

Figure 9. Molecular Viscosity (kg/m-s) contours for Re#15000, eccentricity (5.15 mm), inner rotation (300 RPM) and outer cylinder fixed

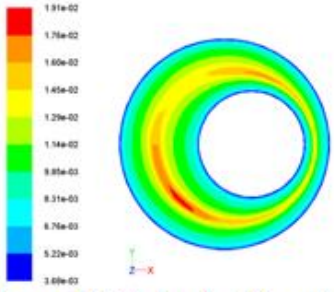

Figure 10. Molecular Viscosity (kg/m-s) contours for Re#15000, eccentricity (5.15 mm), inner rotation (600 RPM) and outer cylinder fixed

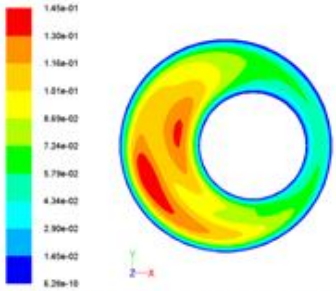

Figure 11. Turbulent Viscosity (Kg/m-s) contours for Re#15000, eccentricity (5.15 mm), inner rotation (300 RPM) and outer

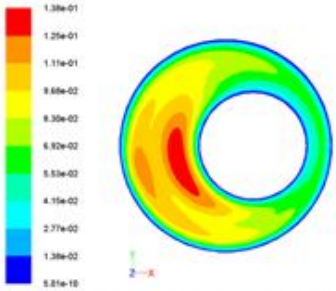

Figure 12. Turbulent Viscosity (kg/m-s) contours for Re#15000, eccentricity (5.15 mm), inner rotation (300 RPM) and outer cylinder fixed

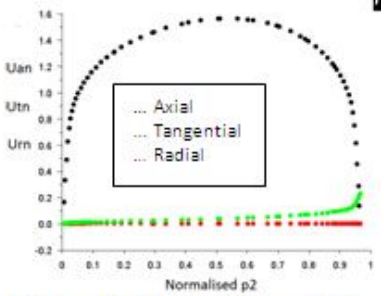

Figure 13. Axial, Tangential and Radial Velocity variation along p2 plane for Re#15k, 600 RPM inner cylinder rotation

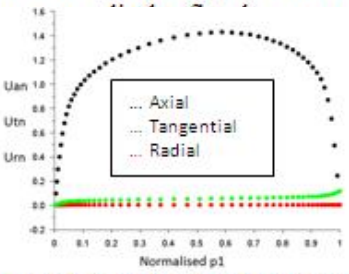

Figure 14. Axial, Tangential and Radial Velocity variation along p1 plane for Re#15k, 300 RPM inner cylinder rotation

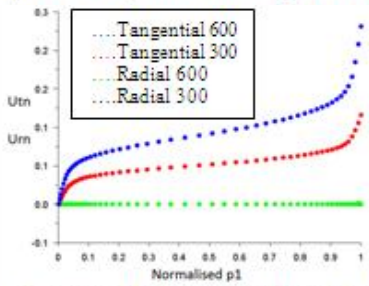

Figure 15. Tangential and Radial velocity variation along p1 for Re#15k, 300 RPM & 600 RPM inner cylinder rotation

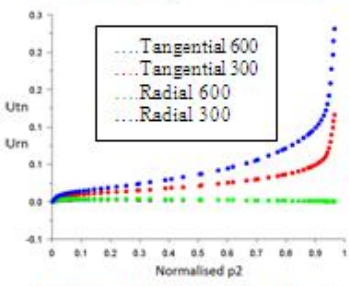

Figure 16. Tangential and Radial velocity variation along p2 for Re#15k, 300 RPM & 600 RPM inner cylinder rotation

IPASJ International Journal of Mechanical Engineering (IIJME)
Web Site: http://www.ipasj.org/IIJME/IIJME.htm
A Publisher for Research Motivation.....
Email: editoriijme@ipasj.org
Volume 3, Issue 8, August 2015
ISSN 2321-6441

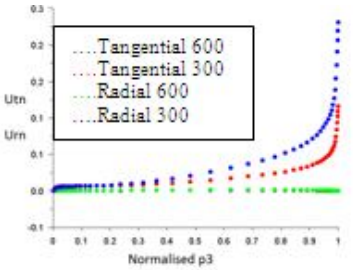

Figure 17. Tangential and Radial velocity variation along p3 for Re# 15k, 300 RPM & 600 RPM inner cylinder rotation

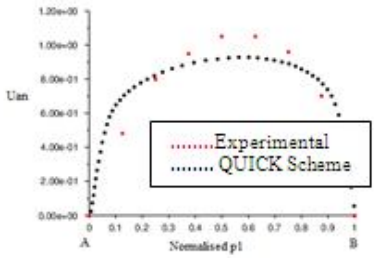

Figure 18. Comparison between experimental & results obtained for Axial velocity variation along p1

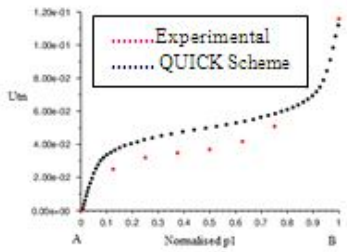

Figure 19. Comparison between experimental & results obtained for Tangential velocity variation along p1

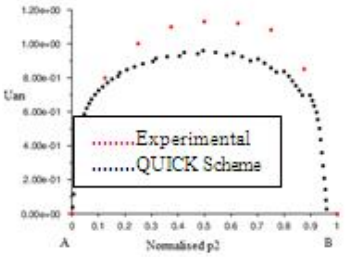

Figure 20. Comparison between experimental & results obtained for Axial velocity variation along p2

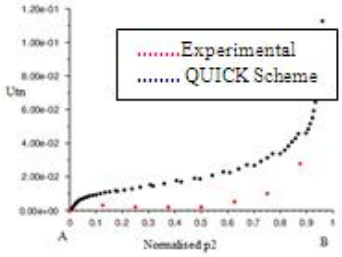

Figure 21. Comparison between experimental& results obtained for Tangential velocity variation along p2

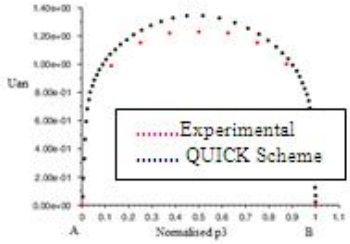

Figure 22. Comparison between experimental& results obtained for Axial velocity variation along p3

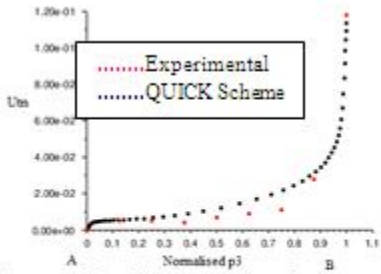

Figure 23. Comparison between experimental & results obtained for Tangential velocity variation along p3